Preprint, accepted for publication in the Proceedings of the Combustion Institute, August 10th 2022.
Presented at the 39th International Symposium on Combustion, Vancouver, BC Canada, July 25th 2022.
Published version and supplemental material available at: https://doi.org/10.1016/j.proci.2022.08.054

Statistical Analysis of Detonation Wave Structure

Mark D. Frederick[a,*], Rohan M. Gejji[a], Joseph E. Shepherd[b], Carson D. Slabaugh[a]

[a] *Purdue University, West Lafayette, IN 47907*
[b] *California Institute of Technology, Pasadena, CA 91125*

Abstract

Hydrocarbon fueled detonations are imaged in a narrow channel with simultaneous schlieren and broadband chemiluminescence at 5 MHz. Mixtures of stoichiometric methane and oxygen are diluted with various levels of nitrogen and argon to alter the detonation stability. Ethane is added in controlled amounts to methane, oxygen, nitrogen mixtures to simulate the effects of high-order hydrocarbons present in natural gas. Sixteen unique mixtures are characterized by performing statistical analysis on data extracted from the images. The leading shock front of the schlieren images is detected and the normal velocity is calculated at all points along the front. Probability distribution functions of the lead shock speed are generated for all cases and the moments of distribution are computed. A strong correlation is found between mixture instability parameters and the variance and skewness of the probability distribution; mixtures with greater instability have larger skewness and variance. This suggests a quantitative alternative to soot foil analysis for experimentally characterizing the extent of detonation instability. The schlieren and chemiluminescence images are used to define an effective chemical length scale as the distance between the shock front and maximum intensity location along the reaction front. Joint probability distribution functions of shock speed and chemical length scale enable statistical characterization of coupling between the leading shock and following reaction zone. For more stable, argon dilute mixtures, it is found that the joint distributions follow the trend of the quasi-steady reaction zone. For unstable, nitrogen diluted mixtures, the distribution only follows the quasi-steady solution during high-speed portions of the front. The addition of ethane is shown to have a stabilizing effect on the detonation, consistent with computed instability parameters.

Keywords: detonation; statistical analysis; instability; imaging

1. Introduction

Detonations are characterized by spatial and temporal fluctuations in the leading shock front and secondary shocks moving transverse to the main front. These features are responsible for the quasi-periodic cellular structures in flow properties and the iconic diamond-shaped cells on soot foils. More importantly, these fluctuations in shock wave motion are nonlinearly coupled to the chemical reaction processes that sustain the detonation wave. In highly unstable detonations, these reaction processes either occur through shock-induced ignition or turbulent mixing in shear flows, which are created by transverse wave and lead shock interaction. The relative importance of these two reaction processes is an ongoing area of research [1–6]. In order to understand how the reaction fields couple with the leading shock wave, it is first necessary to be able to study these two separately to then understand their interplay.

Numerical models and experiments each face unique challenges in accomplishing this goal. Despite significant advances in numerical modeling of detonations, the fidelity needed to investigate issues that involve turbulence while at the same time resolve chemical reactions remains elusive [7, 8]. Equally daunting is the challenge of experimentally resolving shock waves, turbulence, and chemical reactions with sufficient resolution to move beyond qualitative visualization to create quantitative characterization of the fluctuations using statistical methods. There are two major challenges for experimentally characterizing the turbulent flow and chemical reactions in detonations. First is the need to resolve and record the high-speed shock and fluid motion. Second is the simultaneous recording of chemical species or evidence of chemical reaction. For shock wave and fluid motion visualization, schlieren imaging has been the go-to method for a number of generations. The advancement of high-speed imaging systems has now enabled sequences of digital images to be acquired with interframe times as low as 50 ns. However, different techniques such as PLIF [1] or imaging of the chemiluminescence (spontaneous emission of excited radical species) are needed to directly visualize the chemical activity.

Statistical analysis of the leading shock front has been used to study the fluctuating nature of the leading shock speed in both numerical and experimental work for a limited number of mixtures. Using data from 2D numerical simulations, Austin [9] and Shepherd [10] both studied hydrogen-oxygen mixtures and Radulescu *et al.* [2] studied methane-oxygen mixtures. By generating frequency distributions of the lead shock speed sampled in time, all found that the wave tended toward velocities below U_{CJ}. This is reconciled by the fact that the shock spends more time decaying than amplifying. Shepherd also considered the reaction front and generated joint distributions showing how induction length and velocity relate to the quasi-steady prediction. The only authors to have analyzed experimental data, Maxwell *et al.* [5] generated velocity distributions of a methane-oxygen mixture (P_0 = 3.5 kPa, $U_{avg} = 0.82U_{CJ}$) using schlieren images captured with an inter-frame time of 11 μs. Like the numerical models, they found that the distribution skewed toward slower speeds.

In this paper we use a narrow detonation channel together with simultaneous high-speed schlieren and broadband chemiluminescence to create time series of images. The images are at sufficiently high resolution and framing rates to enable robust statistical analysis that builds on and advances the state of art [2, 5, 9, 10] in statistical analysis. The image data were used to compute probability distributions of fluctuations in leading shock speed and joint distributions of reaction front location relative the leading shock. The mixture compositions were varied to obtain a range of instability characteristics and examine the effect on the distribution functions. Comparisons with quasi-steady reaction zone models are used to make inferences about the coupling between fluid mechanics and chemistry.

2. Experiment Description

2.1. Detonation Channel

Experiments were carried out in the *Narrow Channel Facility* (NCF), a high-aspect ratio rectangular channel (152.4 x 17.78 mm) that was developed at the Explosion Dynamics Laboratory at Caltech [9] and is now operated at Zucrow Laboratories. Detonations of premixed gases are directly initiated with an acetylene-oxygen driver at vacuum conditions (22 kPa), which generates a large spatial structure that is advantageous for optical visualization. Loading of reactants is accomplished using the method of partial pressures and monitored by a pressure transducer with an accuracy of 100 Pa. Detailed information regarding the design, operation, and previous findings of the experiment can be found in these studies [9, 11–13].

2.2. Diagnostics

Simultaneous schlieren and broadband chemiluminescence imaging measurements were performed at a rate of 5 MHz. Broadband chemiluminescence was selected to image the reaction field because it enabled images to be captured without the use of an image intensifier, which would limit the dynamic range of the measurement. It also allowed enough light to be captured during the 110 ns exposure time to yield a suitable signal-to-noise ratio. The imaging region was located 3.1 m from the point of initiation and imaged through two 170 mm quartz windows using two Shimadzu HPV-X2 cameras. The schlieren system consists of a pulsed LED source, two f/10 parabolic mirrors, a bandpass filter centered around the LED emission spectra (Semrock FF01-640/20 BrightLine), a circular schlieren cutoff, and a custom camera lens. The camera used for broadband chemiluminescence

imaging was outside of the schlieren beam path, angled at 9° to have a coincident field of view with the schlieren camera. Spatial calibration was performed using DaVis 8.4.0 to correct for the perspective introduced by the angled camera and to precisely overlay the schlieren and chemiluminescence images. The Shimadzu HPV-X2 detectors have a sensor size of 250 x 400 pixels. In this configuration, the field of view was 68 x 108 mm, yielding a spatial resolution is 3.7 pixels/mm.

2.3. Test Conditions

Listed in Table 1 are three different mixture sets that were studied in this work. The first two sets are stoichiometric methane and oxygen diluted with nitrogen or argon. The dilution amount varies from no dilution to the maximum dilution, such that any additional dilution would result in a failed detonation at these initial conditions. The third set consists of blends of methane and ethane with a fixed amount of oxygen and nitrogen. This set is meant to study the sensitivity of natural-gas-like mixtures to ethane concentration. For all cases the initial pressure and temperature were held constant at P_0 = 22.3 kPa and T_0 = 295 K, respectively. Each case was repeated at least twice. The maximum variance in composition across all cases from a desired mixture is 1.6%. The uncertainly of mixture composition and initial pressure is 0.08% and is based on the reported uncertainty of the pressure transducer used to monitor reactant loading.

Also listed in Table 1 are selected detonation parameters that were computed [14] using the CJ-ZND model with the GRI3.0 reaction mechanism [15]. The reported table values are the computed Chapman-Jouguet velocity (U_{CJ}), the induction length (Δ_I), the ratio of the induction length to the exothermic length (Δ_I/Δ_E), and the reduced activation energy (θ). The last two of these parameters are used as predictors of detonation stability and generally speaking, the larger these value are, the more unstable the mixture. A table with additional detonation parameters for these mixtures is provided in the supplemental material (Table S1).

Table 1: Calculated detonation parameters for mixtures tested with P_0 = 22.3 kPa and T_0 = 295 K [14].

x	U_{CJ} [m/s]	Δ_I [mm]	Δ_I/Δ_E	θ
CH_4-2O_2-$x$$N_2$				
0	2325	1.08	16.5	10.5
0.5	2233	1.71	19.65	10.88
1	2164	2.52	22.56	11.21
1.5	2109	3.57	25.77	11.54
2	2062	4.92	29.39	11.86
CH_4-2O_2-xAr				
0.5	2190	1.09	14.06	10.34
1	2094	1.12	12.43	10.21
1.5	2022	1.15	11.27	10.12
2	1965	1.19	10.25	10.00
2.5	1918	1.24	9.53	9.91
(1-x)CH_4-$x$$C_2H_6-2O_2-1.5N_2$				
0.03	2116.8	2.27	16.69	11.49
0.05	2122	1.91	13.96	11.21
0.075	2129	1.59	11.66	10.89
0.1	2134	1.37	10.03	10.62
0.2	2159	0.91	6.58	9.948
0.3	2181	0.70	4.94	9.633

3. Results and Analysis

3.1. Velocity Computation

A time series of the images captured in the work is shown in Fig. 1 for a mixture of CH_4-2O_2-1.5N_2. The broadband chemiluminescence (colored red) is superimposed on the schlieren (colored gray). Images are acquired every 200 ns, but only 8 of the 256 images are included in Fig. 1. The video for this case is provided in the supplemental material (Video S1). Examination of this video is highly encouraged to fully appreciate the evolution of the features within the detonation.

These images allow for the detonation to be understood in terms of the coupled gas-dynamic and reactive components. For example, in portions of the wave where the leading front is fast, up to 1.5U_{CJ}, such as immediately following a transverse wave collision (feature i), the chemiluminescence intensity is high and the intensity peak is located close to the shock front. Whereas, in decaying regions of the front, where the lead shock is slower (feature ii), and the wave speed is as low as 0.6U_{CJ}, the chemiluminescence intensity is much lower and the intensity peak is located further from the shock front. Of particular interest in highly unstable detonations is how this extreme variation in shock speed correlates to the formation of incompletely reacted gas pockets behind the front. The low speed portions of the leading front are not strong enough to promptly initiate rapid reaction. The mechanism of subsequent reaction and role in detonation propagation is an active research question [2, 4]. The formation of a high-density gas pocket can be seen developing (feature iii), separating from the front upon transverse wave collision (feature iv), and dissipating behind the front (feature v).

In order to compute the velocity of the leading front, the first step is to accurately identify and extract the position of the leading front in each frame. This operation is performed on the schlieren images and each image is treated independently. An image is only considered if the leading front encompasses the entire height of the frame. This serves to eliminate any images that have leading fronts that enter or exit the field of view while the camera is acquiring. The images are background subtracted with a reference image to remove slight defects in the windows that are made apparent by the sensitive schlieren system. No other processing steps to handle image imperfections/noise, such as thresholding or smooth-

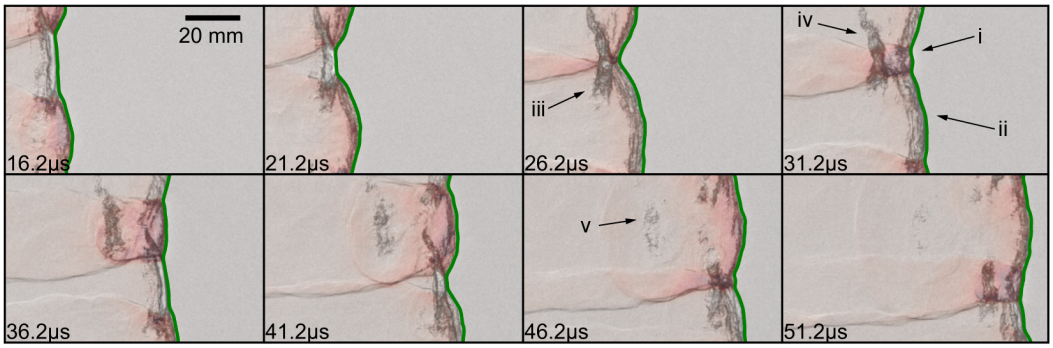

Fig. 1: Simultaneous schlieren and broadband chemiluminescence images of a CH_4-$2O_2$-$1.5N_2$ detonation; every 25th image in the series is shown to illustrate dynamics in 8 frames. The dimension of each image is 68 x 108 mm and a 20 mm scale is shown in the first frame. The detected leading edge of the shock front is shown as a green line.

ing, are required. The background subtracted images are then processed with a horizontal Sobel filter to approximate the spatial gradient in the direction that the wave travels, which serves to emphasize the discontinuity in intensity caused by the shock. Moving one pixel at a time along the vertical direction of the image, the horizontal position of the minimum value of the spatial gradient is recorded as the front location. This yields 250 front locations per image. These locations are further refined using an active contour model, which also has the effect of smoothing the edge. The extracted leading front is overlaid on the images in Fig. 1 as a green line.

The leading shock front, especially for cases of high instability, is often curved. Therefore the normal velocity is calculated and considered in this work. At each front location, the spatial gradient is found using a 2nd order accurate central-difference for interior points and forward-difference for exterior points to define the normal vector. The normal velocity at each front point is then found using the same finite difference schemes as above, except that the derivative is found in time (between frames) instead of space. The points from neighboring fronts needed to compute the derivative are found along the normal vector of the front location under consideration using cubic spline interpolation. Any outliers, defined as being greater than $2U_{CJ}$, are eliminated.

A velocity map is an image where the computed velocity is normalized by U_{CJ} at each front location, cast onto a color scale, and plotted at its extracted spatial location. The spatial structure described by such a representation is similar to what might be obtained from a soot foil. However, in addition to spatial information the velocity map also shows a history of the instantaneous lead shock velocity. A representative velocity map is shown in Fig. 2a for a mixture of $2H_2$-O_2-$8N_2$ initiated at the same conditions as in Table 1. This mixture was chosen as a baseline, to validate the processing methodology and outcomes with rigorous characterizations performed in prior works [9, 10]. The cellular structure is spatially periodic and clearly visible. At the beginning of each cell cycle, which is the moment directly following transverse wave collision, the lead shock is accelerated and its velocity is increased to super-U_{CJ} speeds before the front decays to sub-U_{CJ} speeds. Following another transverse wave collision, the front re-accelerates and another cell cycle begins. This pattern is made apparent in the velocity map where the cell cycle begins with a region of high intensity red and then gradually fades to blue as the shock speed decays.

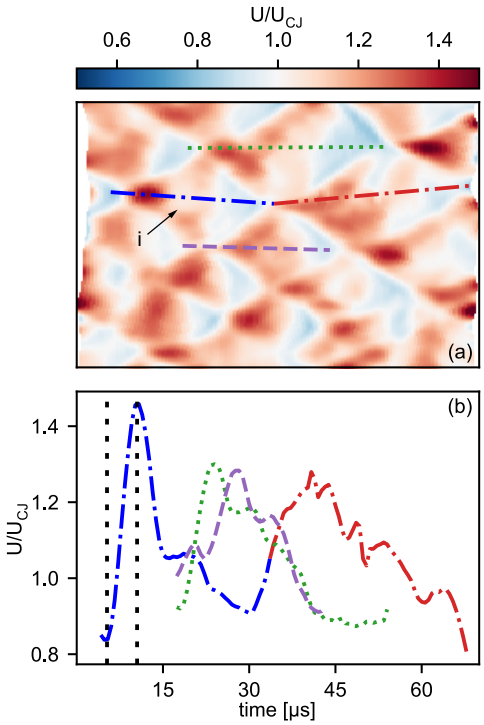

Fig. 2: a) Normalized velocity map of a $2H_2$-O_2-$8N_2$ detonation with U_{CJ} = 1653 m/s, Δ_I = 3.99 mm, Δ_I/Δ_E = 4.66, θ = 8.52 and b) cell centered velocity profiles extracted from (a).

Figure 2b further investigates the center-line veloc-

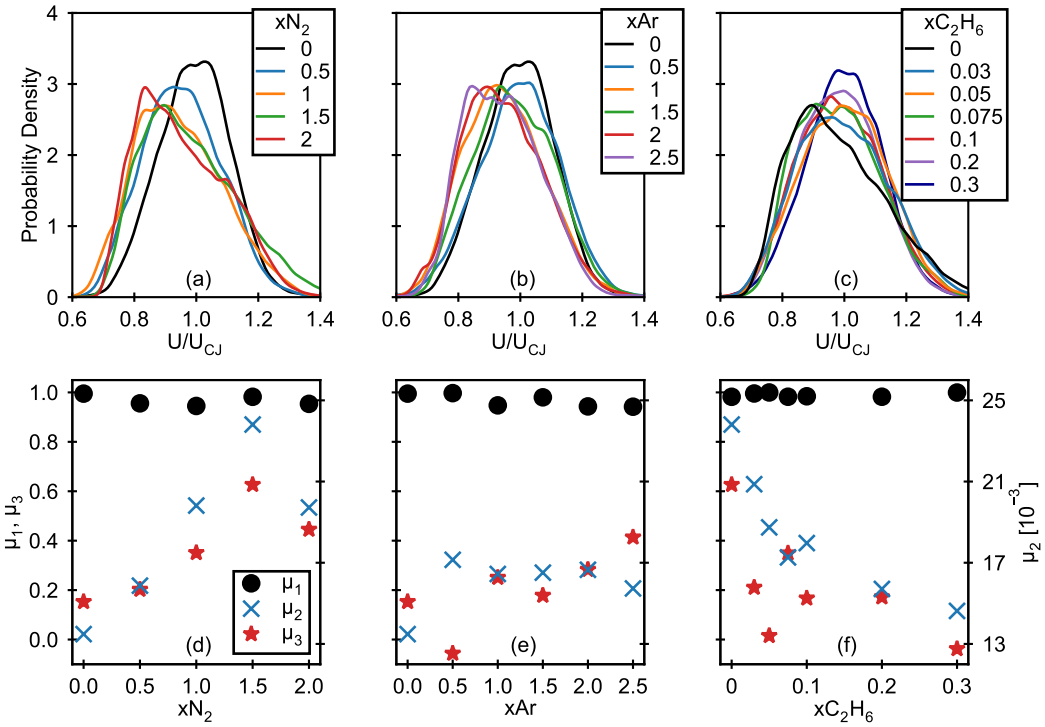

Fig. 3: Leading front normal velocity probability density functions (a,b,c) and the first three moments of distribution (d,e,f) for mixtures of (a,d) CH_4-2O_2-$x$$N_2$, (b,e) CH_4-2O_2-xAr, and (c,f) (1-x)CH_4-$x$$C_2H_6-2O_2-1.5N_2$. The moments of distribution are the μ_1: mean, μ_2: variance, and μ_3: skewness.

ity profiles of four cells that were selected from the velocity map in Fig. 2a. These velocities are computed along the direction of the superimposed lines. At the beginning of each profile the wave accelerates rapidly and then decays for the remainder of the cycle. The amount of time that the wave spends accelerating along profile (i) is demarcated with the dotted vertical lines in Fig. 2b and amounts to 21% of the cell cycle time. This acceleration period is well resolved, with 10 sample points. For the remainder of this work individual velocity profiles will not be considered and instead the amalgamation of all computed velocities will be analyzed statistically.

3.2. Statistical Analysis of Leading Front Velocity

The leading front can be analyzed statistically to characterize its fluctuating properties. Probability density functions (PDFs) of the leading front normal velocity sampled in time are shown in Fig. 3(a,b,c) for all cases listed in Table 1. The PDFs were generated using a kernel density estimate. In order to ensure that these PDFs contain enough sample points of complete cell cycles to statistically represent a given mixture, at least two sets of images were used to generate each. This is particularly important for the highly dilute cases that generate large cells, such as the one shown in Fig. 1. Each PDF is generated from at least 110,000 sample points.

Figure 3 (a) and (b) shows the PDFs for CH_4-2O_2 mixtures diluted with various amounts of nitrogen and argon, respectively. For both mixture sets, the shape of the PDFs appears to be nearly symmetric about U/U_{CJ} = 1 for low levels of dilution. But, as dilution is increased the shape of the PDFs take on a different character for the different diluents. For the nitrogen cases (a), the PDFs become less symmetric and skew toward sub-U_{CJ} speeds. While for the argon cases (b), the bulk of the PDFs appear to shift toward slower speeds, but the symmetry of the distributions does not change as drastically as it does for the cases in (a). These trends can be understood quantitatively by examining the first three moments of distribution, which are plotted in Fig. 3 (d) and (e) for these cases. The mean value (μ_1) decreases for both nitrogen and argon mixtures as the amount of dilution is increased. For example in the case of argon (e), at x = 0, μ_1 = 0.995 and at x = 2.5, μ_1 = 0.942. Distinctions between the two mixtures sets can be found by considering the variance (μ_2) and the skewness (μ_3). The variance measures how far the data set is spread from the mean and the skewness measures the asymmetry of the data. As the amount of dilution is increased in (d), both the variance and skewness increase. However, as dilution is increased in (e) the variance and

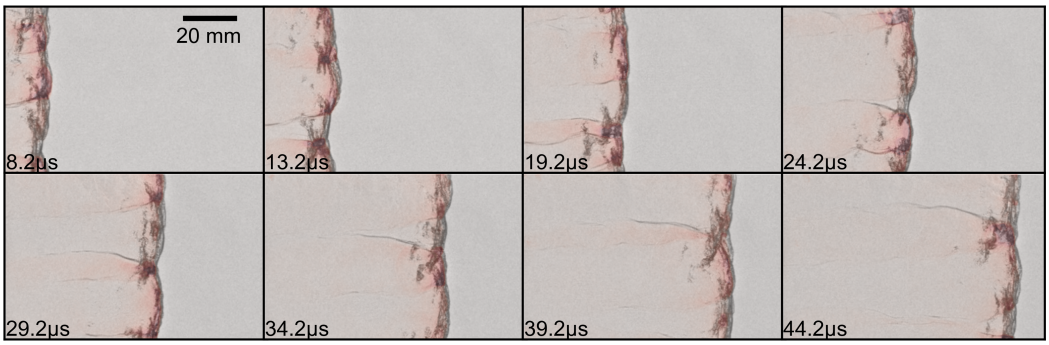

Fig. 4: Sequence of simultaneous schlieren and broadband emission images of a $0.95CH_4$-$0.05C_2H_6$-$2O_2$-$1.5N_2$ detonation; every 25th image in the series is shown to illustrate dynamics in 8 frames. The dimension of each image is 108 x 68 mm and a 20 mm scale is shown in the first frame.

skewness remain nearly constant.

Nitrogen dilution, as compared to argon, creates a larger spread in the front velocity and also shifts the mass of the distribution further toward sub-U_{CJ} speeds, which means that the wave spends more time moving slower than the mean velocity. These trends in variance and skewness can be physically explained by considering the detonation front stability properties of these mixtures. As the concentration of nitrogen increases, the instability increases, but as the concentration of argon increases, the instability decreases. Two values used to quantify instability are Δ_I/Δ_E and θ, which are provided in Table 1. Taking the ratio of these parameters at x = 0 and x = 2 results in Δ_I/Δ_E and θ increasing by a factor of 1.78 and 1.13, respectively, for nitrogen, and Δ_I/Δ_E and θ decreasing by a factor of 0.67 and 0.96, respectively, for argon. Analysis [16, 17] of the steady ZND reaction zone structure of acetylene/oxygen mixtures reveals the mechanism of reducing detonation instability by argon addition. Increasing argon concentration increases the postshock temperature (for less than 70% argon); reducing the peak energy release rate, Δ_I/Δ_E, and θ. These effects render the detonation front more stable, consistent with experimental observations.

Figure 3 (c) and (f) show the effect that increasing the concentration of ethane has on the lead front velocity for mixtures of $(1\text{-}x)CH_4$-xC_2H_6-$2O_2$-$1.5N_2$. The total mole fraction of fuel is held constant and the relative amounts of methane and ethane are varied from 0-30% ethane. As the concentration of ethane is increased the PDFs skew rightward. This is supported by the moments in (f). Both the variance and skewness decrease as the concentration of ethane is increased. A decrease in variance means that the velocity spread is held closer to the mean value. A decrease in skewness means that the mass of the distribution moves rightward and the right tail of the distribution becomes smaller, indicating that less extreme super-U_{CJ} velocities occur. These factors all indicate that the introduction of ethane has a stabilizing effect on the mixture, reducing the magnitude of the velocity oscillations of the front. This is supported by the stability parameters Δ_I/Δ_E and θ that are shown in Table 1.

The presence of even a small amount of ethane has the effect of dramatically reducing the induction length of a mixture that is primarily fueled with methane. This result was discovered by Westbrook [18], who was interested in why natural gas-air was more detonable that methane-air mixtures. Using a detailed kinetic mechanism, Westbrook and Haselman [19] demonstrated that ethane sensitizes the mixture because it more easily undergoes hydrogen abstraction, promoting chain branching reactions and avoiding the kinetic bottleneck of methyl radical production. The exothermic length is relatively unchanged by ethane addition and decreasing the induction length relative to the exothermic length (smaller Δ_I/Δ_E) is known [20] to be correlated with increasing the stability of the detonation front, consistent with the observed trend in the present data.

In order to compare the structural differences that occur due to the addition of ethane, a time series of images is provided in Fig. 4 for a mixture of $0.95CH_4$-$0.05C_2H_6$-$2O_2$-$1.5N_2$. This mixture is diluted with the same amount of nitrogen as the case shown in Fig. 1, which is fueled with pure methane. The leading front of Fig. 4 has much less curvature and more triple point crossings than Fig. 1. Additionally, no large structures, such as the detached gas pocket (feature (v) in Fig 1) exist far behind the front. Since the instability, and therefore shock speed variation, has decreased with the addition of ethane, fewer regions of extreme sub-U_{CJ} speeds are present along the front resulting in fewer regions of low chemical activity far behind the front..

3.3. Joint Probability Distributions

To fully capture the processes occurring along the leading shock, both the gas dynamic and chemical aspects must be examined. Unsteadiness in velocity of the front correlates with unsteadiness in the reaction structure. This can seen through the images in Fig. 1

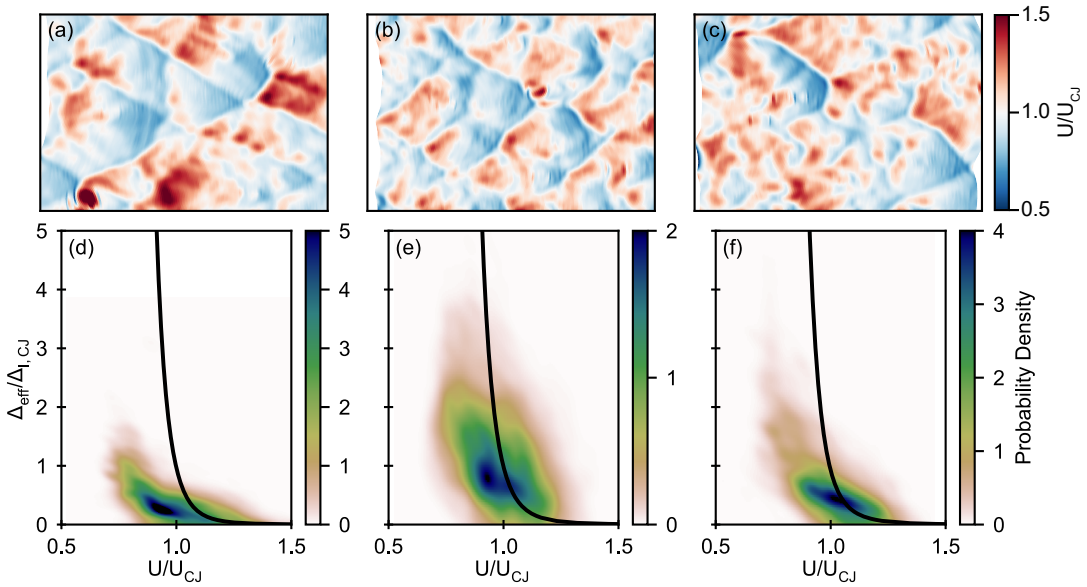

Fig. 5: Normalized velocity map (a,b,c) and joint probability distribution functions of normalized velocity and effective chemical length (d,e,f) for mixtures of (a,d) CH_4-$2O_2$-$1.5N_2$, (b,e) CH_4-$2O_2$-1.5Ar, and (c,f) $0.95CH_4$-$0.05C_2H_6$-$2O_2$-$1.5N_2$. The quasi-steady reaction zone is plotted as a black line in each of (d,e,f).

and 4. In order to statistically characterize the relationship between the front velocity and the reaction front, we compute an effective chemical length scale (Δ_{eff}) using the broadband chemiluminescence images to generate the joint PDFs shown in Fig. 5. Δ_{eff} is a measure of the distance from the shock front to the reaction front and is computed by first extracting an edge from each broadband chemiluminescence image along the location of maximum intensity close to the leading front. This is done by thresholding each image. While we recognize that broadband chemiluminescence is not a species specific measurement, it is commonly used in the combustion community as a marker of heat release [4, 5, 21, 22]. An example of the extracted edge is shown for a single frame in Fig. 6. To compute Δ_{eff}, the difference between the shock front edge and reaction front edge is found along the normal of the shock front edge. Δ_{eff} is then normalized by the ZND induction length computed at U_{CJ} in order to compare with the normalized velocity U/U_{CJ}.

The joint PDFs of normalized velocity and Δ_{eff} are shown in Fig. 5(d,e,f) for three mixtures. The quasi-steady reaction zone length is calculated using the constant-pressure explosion model and superimposed on the PDFs as a black line. Also provided in Fig. 5(a,b,c) are representative normalized velocity maps for the mixtures shown in the joint PDFs. Videos, S2 and S3, are provided in the supplemental material for the cases shown in (b) and (c), respectively. The case shown in (e), CH_4-$2O_2$-1.5Ar, is the most stable of the three and its distribution most closely follows the quasi-steady solution, although it is clearly shifted to the left. The CH_4-$2O_2$-$1.5N_2$ mixture, shown in (d), has a much different behavior than (e). The distribution only follows the quasi-steady solution during high speed periods. At low speeds the distribution favors smaller induction lengths. The case in (f) is the same mixture as in (d), except that 5% of the fuel is ethane. The distribution is more localized around the quasi-steady solution near U/U_{CJ} = 1, as compared to (d). Additionally, in the low speed regions the trend begins to more closely follow the quasi-steady solution. These results support the conclusion drawn by Liang and Shepherd [10], who performed a similar analysis with numerical data. Highly unstable mixtures, as shown here, only conform to the quasi-steady solution during high speed portions of the wave front. During low speed portions, the wave front must be treated as fully unsteady.

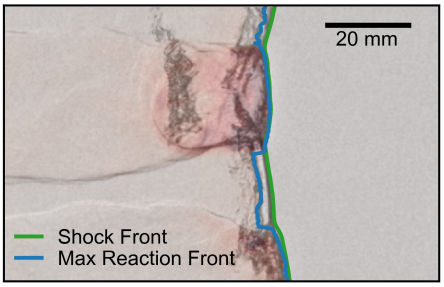

Fig. 6: Extracted shock front and maximum reaction front edge for a single frame of a CH_4-$2O_2$-$1.5N_2$ detonation.

4. Conclusion

We performed a quantitative analysis on simultaneous schlieren and broadband chemiluminescence images obtained at 5 MHz in a narrow detonation channel. Methane, oxygen mixtures were diluted with various amounts of nitrogen or argon to change the mixture stability. Between 3-30% ethane (by fuel volume) was added to methane, oxygen, nitrogen mixtures to study the stabilizing role that ethane plays in natural gas detonations. Using statistical methods, we characterized the oscillatory nature of both the shock and reaction fronts of these mixtures. We have demonstrated how trends in distribution functions and moments reflect changes in detonation front stability with varying mixture composition. Velocity distribution skewness is positively correlated with detonation front instability as determined from visual observation and computed reaction zone parameters θ and Δ_E/Δ_I. The joint distributions of experimental velocity and effective reaction zone thickness fluctuations demonstrate the dramatic effects of mixture composition on the extent of coupling between the energy release zone and shock front. Comparisons of the joint distribution functions with the predictions of a quasi-steady reaction zone model are consistent with the findings of prior work. These results demonstrate the value of this experimental methodology in quantitatively describing detonation front instability and point the way to furthering our understanding of the coupling between chemical kinetics and fluid mechanics that powers the instability.

Acknowledgments

This work was supported by U.S. Air Force Office of Scientific Research grant FA9550-21-1-0013 (PO: Dr. Chiping Li). Mark D. Frederick acknowledges support from the National Science Foundation Graduate Research Fellowship Program under Grant No. DGE-1333468. One Shimadzu HPV-X2 used in this work was purchased with DURIP grant FA9550-20-1-0226 (PO: Dr. Chiping Li). The authors are grateful to Hadland Imaging for use of the second Shimadzu HPV-X2.

Supplementary material

Supplementary material associated with this article can be found in the online version.

References

[1] F. Pintgen, C. A. Eckett, J. M. Austin, J. E. Shepherd, Direct observations of reaction zone structure in propagating detonations, Combust. Flame 133 (3) (2003) 211–229.

[2] M. I. Radulescu, G. J. Sharpe, C. K. Law, J. H. Lee, The hydrodynamic structure of unstable cellular detonations, J. Fluid Mech. 580 (2007) 31–81.

[3] S. R. Sanderson, J. M. Austin, Z. Liang, F. Pintgen, J. E. Shepherd, H. G. Hornung, Reactant jetting in unstable detonation, Prog. Aerosp. Sci. 46 (2-3) (2010) 116–131.

[4] C. B. Kiyanda, A. J. Higgins, Photographic investigation into the mechanism of combustion in irregular detonation waves, Shock Waves 23 (2013) 115–130.

[5] B. M. Maxwell, R. R. Bhattacharjee, S. S. M. Lau-Chapdelaine, S. Falle, G. J. Sharpe, M. I. Radulescu, Influence of turbulent fluctuations on detonation propagation, J. Fluid Mech. 818 (2017) 646–696.

[6] A. Sow, S. M. Lau-Chapdelaine, M. I. Radulescu, The effect of the polytropic index γ on the structure of gaseous detonations, Proc. Combust. Inst. 38 (3) (2021) 3633–3640.

[7] J. M. Powers, Review of Multiscale Modeling of Detonation, J. Propuls. Power 22 (6) (2006) 1217–1229.

[8] M. I. Radulescu, A detonation paradox: Why inviscid detonation simulations predict the incorrect trend for the role of instability in gaseous cellular detonations?, Combust. Flame 195 (2018) 151–162.

[9] J. M. Austin, The Role of Instability in Gaseous Detonation, Ph.D. thesis, California Institute of Technology (2003).

[10] J. E. Shepherd, Detonation in gases, Proc. Combust. Inst. 32 (1) (2009) 83–98.

[11] J. M. Austin, J. E. Shepherd, Detonations in hydrocarbon fuel blends, Combust. Flame 132 (1-2) (2003) 73–90.

[12] J. M. Austin, F. Pintgen, J. E. Shepherd, Reaction zones in highly unstable detonations, Proc. Combust. Inst. 30 (2) (2005) 1849–1857.

[13] M. D. Frederick, R. M. Gejji, J. E. Shepherd, C. D. Slabaugh, Preliminary Results from Narrow Channel Facility Experiments at Purdue University, in: AIAA Propulsion and Energy Forum, 2019.

[14] J. E. Shepherd, Shock and Detonation Toolbox (2018). URL `shepherd.caltech.edu/SDT/`

[15] G. P. Smith, D. M. Golden, M. Frenklach, M. W. Moriarty, B. Eiteneer, M. Goldenberg, C. T. Bowman, R. K. Hanson, S. Song, W. C. Gardiner, V. V. Lissianski, Z. Qin, GRI-Mech (Jul. 1999). URL `www.me.berkeley.edu/gri_mech/`

[16] J. E. Shepherd, I. O. Moen, S. B. Murray, P. A. Thibault, Analyses of the Cellular Structure of Detonations, Proc. Combust. Inst. 21 (1986) 1649–1658.

[17] M. Radulescu, H. Ng, J. Lee, B. Varatharajan, The effect of argon dilution on the stability of acetylene/oxygen detonations, Proc. Combust. Inst. 29 (2) (2002) 2825–2831.

[18] C. K. Westbrook, An Analytical Study of the Shock Tube Ignition of Mixtures of Methane and Ethane, Combust. Sci. Technol. 20 (1-2) (1979) 5–17.

[19] C. K. Westbrook, L. C. Haselman, Chemical Kinetics in LNG Detonations, in: 7th ICOGER, American Institute of Aeronautics and Astronautics, Inc., Göttingen, 1979, pp. 193–206.

[20] H. Ng, M. Radulescu, A. Higgins, N. Nikiforakis, J. Lee, Numerical investigation of the instability for one-dimensional Chapman-Jouguet detonations with chain-branching kinetics, Combust. Theory Model. 9 (3) (2005) 385–401.

[21] M. J. Bedard, T. L. Fuller, S. Sardeshmukh, W. E. Anderson, Chemiluminescence as a diagnostic in studying combustion instability in a practical combustor, Combust. Flame 213 (2020) 211–225.

[22] J. Ballester, R. Hernández, A. Sanz, A. Smolarz,

J. Barroso, A. Pina, Chemiluminescence monitoring in premixed flames of natural gas and its blends with hydrogen, Proc. Combust. Inst. 32 II (2) (2009) 2983–2991.